ELSEVIER

Comput. Methods Appl. Mech. Engrg. 143 (1997) 349–372

Computer methods in applied mechanics and engineering

A monotone finite element method with test space of Legendre polynomials

Tony W.H. Sheu*, S.F. Tsai[1], Morten M.T. Wang[1]

Department of Naval Architecture and Ocean Engineering, National Taiwan University, 73 Chou-Shan Rd., Taipei, Taiwan, R.O.C.

Received 13 June 1995; revised 17 June 1996

Abstract

This paper is concerned with the development of a multi-dimensional monotone scheme to deal with erroneous oscillations in regions where sharp gradients exist. The strategy behind the underlying finite element analysis is the accommodation of the M-matrix to the Petrov–Galerkin finite element model. An irreducible diagonal-dominated coefficient matrix is rendered through the use of exponential weighting functions. With a priori knowledge capable of leading to a Monotone matrix, the analysis model is well conditioned with the monotonicity-preserving property. In order to stress the effectiveness of test functions in resolving oscillations, we considered two classes of the convection–diffusion problem. As seen from the computed results, we can classify the proposed finite element model as legitimate for the problem free of boundary layer. Also, through the use of this model, we can capture the solution for the problem involving a high gradient. In this study, we are interested in a cost-effective method which ensures monotonicity irrespective of the value of the Peclet number throughout the entire domain. To gain access to these desired properties, it is tempting to bring in the Legendre polynomials and the characteristic information so that by virtue of the inherent orthogonal property the integral can be obtained exactly by two Gaussian integration points along each spatial direction while maintaining stability in the M-matrix satisfaction sense.

1. Introduction

In many physical problems transport is a very important and sometimes even a crucial process. Thus, a linear elliptic partial differential equation governing a steady-state convection–diffusion process is of primary importance in the fields of fluid mechanics, heat transfer and semiconductor device modelling. With the advent of computers, large in capacity, numerical simulation of this class of engineering problem has gained increasing acceptance. While this benchmark problem is regarded as important in itself, from a numerical analysis point of view, its real importance lies in its resemblance to, among others, the linearized Navier–Stokes equations. Simply stated, this problem can be viewed as a simplification of the Navier–Stokes equations and thus subject of interest, academically as well as practically.

Despite several decades of numerical experience, by now, approaches to the construction of advection scheme for the linear scalar transport equation still raised open. Some of them have answers but not yet definite. Severe restrictions on mesh or grid spacing are indispensable when the flow field possesses significant convective effect. An obstacle to finding a satisfactory prediction of the field variable is due mainly to the first derivative terms, especially for problems involving multiple

* Corresponding author. Professor.
[1] Graduate student.

PII S0045-7825(96)01158-9

dimensions under conditions of high Reynolds (or Peclet) numbers. In this regard, considerable attention has been given to circumventing notorious difficulties arising from direction-dependent fluxes.

Simulation quality can be judged from many aspects. What fits for the solution accuracy may not for the solution stability. For instance, the use of an upwind scheme enhances the stability of the discrete system. In situations where the Peclet number is fairly high, the quality of the simulation is unfortunately overshadowed by the addition of a cross-stream diffusion error. These excessive artificial viscosities may over-spread the solution profile and, thus, contaminate the real physics. Poor performance means such methods are hardly applicable to problems involving a steep gradient of the convective field variable. As a result, researchers have attempted to resolve the dilemma of the inability to gain equal success in solution accuracy and stability. A multitude of concepts have been spawned in the literature to alleviate the problem of accuracy deterioration, yet numerical stability is retained. In common, these cures easily hold in one dimension. While this idea is amenable to one-dimensional analysis, one quickly learns through practice that high-resolution solutions thus far obtained are not easily maintained in multiple dimensions. This limitation is mostly due to the lack of a physically plausible approach in distributing influences to the downstream side. Skew upwind [1] and streamline methods [2] have been devised to limit the artificial diffusion to the flow direction. While this helps to stabilize the calculations for smooth flows, the introduced artificial damping is too weak to wipe out the unwanted wiggles in areas where discontinuities or high gradients appear. As is usual in the development of multi-dimensional advective flux schemes, a scheme endowed with higher accuracy is doomed to lose the solution monotonicity property. As a result, we have felt the need for a treatise on this issue.

The finite element method has been applied with good success for years to problems of solid mechanics and heat conduction. When applied to the field of fluid dynamics in the mid 1960s, the finite elements method had a number of attractions. An appealing advantage is its flexibility in managing geometric complexity. Besides these superiorities, the finite element method is more applicable to differential equations involving boundary conditions of the Neumann type. These advantages make the methodology presented herein suitable for simulating a convection–diffusion equation. Petrov–Galerkin finite element methods have been applied with good success to the advection–diffusion equation. Among them, the streamline upwinding version of Hughes and Brooks [3] is currently the most widely used upwind finite element method. Nevertheless, the quality of the SUPG solution deteriorates as discontinuities, a high gradient boundary layer, or an internal sharp layer are encountered. To surmount these spurious oscillations, Mizukami and Hughes [4] modified their original SUPG formulation by forcing the stiffness matrix equations to satisfy the maximum principle [5–7]. This underlying principle plays a key role in offering a monotonic behavior of the solution variable. Instead of modifying the test functions, Rice and Schnipke [8] and Hill and Baskharone [9] took a different approach to arriving at monotonic solution profiles by evaluating the integral involving convection terms along the local streamline. In 1982, Ahués and Telies [5] used an exponential biased test function to yield an M-matrix. This prompts us to adopt their idea and design a weighting function which can similarly offer upstream weighting of a similar sort. In short, the proposed upwinding model is intended to capture high-gradient physical phenomena.

We began by describing in Section 2 the target problem, known as the convection–diffusion equation. We brought in the monotonicity-preserving property to the framework of the Petrov–Galerkin method. Since solution accuracy and stability have great influence on simulation quality, we carried out fundamental studies and discussed them in detail. In order to validate the proposed flux discretization scheme, we have presented the closed-form solution for the scalar transport equation defined in a square cavity. Attention was directed to assessing the scheme performance.

2. Multi-dimensional flux discretization scheme

2.1. Model equation and discretization method

Seeking solutions for the transport equation that is of convection dominance in multiple dimensions has been shown to be a difficult task and has been the subject of much intensive study in the

computational fluid dynamics community. The main reason why this problem has received focal attention is its resemblance to the linearized equations of motion for an incompressible fluid flow. As a model problem, we consider the convection–diffusion equation in a homogeneous medium. For the purpose of brevity, this paper will be restricted only to a simple case having a constant diffusion coefficient μ in a given velocity field $\underline{u} = (u, v)$. In a simply-connected domain D, the solution to the following elliptic partial differential equation is sought:

$$u\Phi_x + v\Phi_y = \mu(\Phi_{xx} + \Phi_{yy}) . \tag{1}$$

In order to close the above differential system, the boundary condition we impose takes the Dirichlet form. Subject to the prescribed boundary values of Φ, the interior finite element solutions $\hat{\Phi}$ are the result of convection and diffusion effects. The relative importance is best estimated by the maximum Peclet number $\mathrm{Pe} = \max(\mathrm{Pe}_x, \mathrm{Pe}_y) = \max((u\,\Delta x)/\mu, (v\,\Delta y)/\mu)$, where Δx and Δy denote mesh sizes along the x and y directions, respectively.

In weighted residuals context, Galerkin-based, collocation, and least-squares methods are well known [10]. Among them, one formulation has an advantage over another only in certain circumstances. In situations where the effect of convection dominates that of diffusion, it is imperative that one consider the upwinding procedures. Following the method of weighted residuals, we dictate that $R = u\hat{\Phi}_x + v\hat{\Phi}_y - \mu(\hat{\Phi}_{xx} + \hat{\Phi}_{yy})$ be orthogonal to the weighting function. The solution sought can be seen as a search for the weak solution to Eq. (1). In the Petrov–Galerkin context, we demand the test space W_i be different from the trial space N_i. By a successive substitution of $\hat{\Phi} = \Sigma\, N_i(\xi, \eta)\Phi_i$ into the weighted residuals statement, we were led to a matrix equation in the 4-node isoparameter bilinear element wherein the bilinear interpolation function N_i is used. Upon assemblage of all the elements, the global coefficient matrix is formed. What remains is the decision on the content of the test space, which is of pivotal importance and a rather obscure issue, before the weak solution can be obtained by using a direct solution solver.

2.2. Construction of test space

As progress has been made in the area of flux discretization, scientists have asked for simultaneous satisfaction of desirable properties: conservativeness, convective stability and boundedness. Upwind finite element models suffice to render the first two properties. The accessibility of the boundedness property is closely related to the coefficient matrix. On the condition that the diagonal dominance, which serves as a sufficient condition for arriving at bounded solutions, holds, non-physical overshoots or undershoots are avoided.

Based on the above reasoning, we resort to using the Petrov–Galerkin formulation. The question remaining is the selection of biased polynomials which can render a monotone solution. We elaborated constructing such a finite element coefficient matrix. Thanks to the work of Ahués and Telies [5], we take the exponential type of weighting functions into consideration since the resulting coefficient matrix tends to be an M-matrix.

We attempt to find a general rule in the hope of obtaining a multi-dimensional monotone solution. Before turning to construction of such a test space, it is convenient to present some useful theorems and definitions [5–7].

DEFINITION 1. A real $n \times n$ matrix $\underline{\underline{A}} = (a_{ij})$ is said to be irreducible diagonally dominant if $|a_{ii}| > \Sigma_{\substack{j=1 \\ j \neq i}}^{n} |a_{ij}|$ for at least one i.

THEOREM 1. If $\underline{\underline{A}} = (a_{ij})$ is a real, irreducible diagonally dominant $n \times n$ matrix with $a_{ij} \leq 0$ for $i \neq j$ and $a_{ii} > 0$ for $1 \leq i \leq n$, then $\underline{\underline{A}}$ is invertible and its inverse has no negative entries (or $\underline{\underline{A}}^{-1} > 0$).

DEFINITION 2. A real $n \times n$ matrix $\underline{\underline{A}} = (a_{ij})$ with $a_{ij} \leq 0$ for all $i \neq j$ is an M-matrix if $\underline{\underline{A}}$ is nonsingular and its inverse of $\underline{\underline{A}}$ has no negative entries (or $\underline{\underline{A}}^{-1} > 0$).

DEFINITION 3. A real $n \times n$ matrix $\underline{\underline{A}}$ is defined to be monotone if $\underline{\underline{A}}\underline{\phi} \geq 0$ holds for any vector $\underline{\phi}$, it implies $\underline{\phi} \geq 0$.

THEOREM 2. If the off-diagonal entries of $\underline{\underline{A}}$ are nonpositive, we are led to a monotone $\underline{\underline{A}}$ if and only if $\underline{\underline{A}}$ is an M-matrix.

In seeking nonoscillatory solutions over a domain that is spanned by multiple dimensions, a priori satisfaction of the monotone matrix equation is of requisite and enables us to predict solutions of high quality over a wide range of flow conditions. In this paper, finite element formulation is the candidate for the space discretization. In the underlying Petrov–Galerkin approach, the test functions are exponential-weighted modifications of the basis functions N_i:

$$W_i = N_i + B_i \,, \tag{2}$$

where

$$B_i(\xi,\eta) = \left[\exp\left(-\frac{\alpha u h_\xi}{2\mu}(\xi - \xi_i) \right) \exp\left(-\frac{\beta v h_\eta}{2\mu}(\eta - \eta_i) \right) - 1 \right] N_i(\xi,\eta) \,, \tag{3}$$

$$N_i(\xi,\eta) = \frac{1}{4}(1 + \xi_i\xi)(1 + \eta_i\eta) \,. \tag{4}$$

In Eq. (3), h_ξ and h_η denote grid sizes. α, β are adjustable constants which are set to be one herein for simplicity.

We have plotted the piecewise weighting function in a square having four bilinear elements. For the reference node (i, j) in Fig. 1, clearly illuminated is the enhanced stability which is directly attributable to the biased exponential polynomial defined in Eq. (3). Without loss of generality, we consider the scalar problem in two dimensions. For extension to three dimensions or to a system of equations, one could follow the same procedures.

2.3. Fundamental study on accuracy

Technical issues regarding the solution stability and accuracy deserve detailed discussion in order to gain insight into the developed advective scheme. Given a priori knowledge of discretization errors, analysts may make a better judgment on the discretization methods for the problem under investigation. In an attempt to reveal the solution accuracy, we were urged to conduct a modified

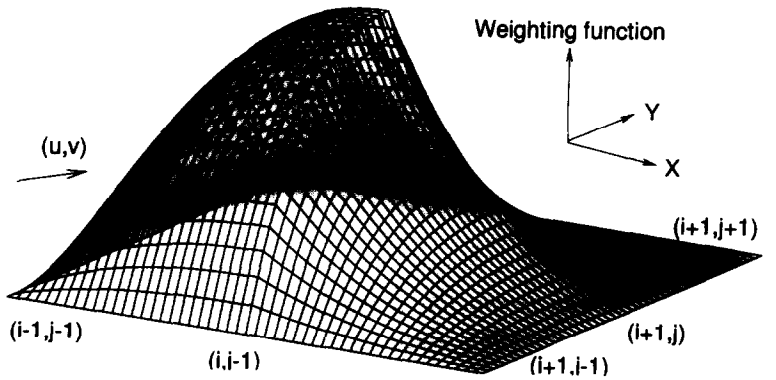

Fig. 1. Weighting function, as defined in Eqs. (2)–(4), in a block of four bilinear elements having a common corner node (i, j).

equation analysis. By taking the standard procedure of Warming and Hyett [11], we can derive the following modified equation for (1):

$$u\Phi_x + v\Phi_y - \mu(\Phi_{xx} + \Phi_{yy}) = T\,, \tag{5}$$

where

$$T = c_1\Phi_{xx} + c_2\Phi_{xy} + c_3\Phi_{yy} + d_1\Phi_{xxx} + d_2\Phi_{yyy} + d_3\Phi_{xxy} + d_4\Phi_{xyy} + e_1\Phi_{xxxx} + e_2\Phi_{xxxy} + e_3\Phi_{xxyy} + e_4\Phi_{xyyy} + e_5\Phi_{yyyy} + \cdots \tag{6}$$

Owing to the use of exponential polynomials, algebraic manipulations to derive the coefficients in Eq. (6) are considerable. This fact precludes the functional representation for these coefficients in Eq. (6). We have plotted three leading coefficients logarithmically against the grid sizes in Fig. 2. The rates of convergence for Φ_{xxxy} and Φ_{xyyy} are $O(h^4)$ while those for Φ_{xy}, Φ_{xxx}, Φ_{yyy}, Φ_{xxy}, Φ_{xyy}, Φ_{xxxx}, Φ_{yyyy} and Φ_{xxyy} are in the vicinity of $O(h^2)$. As to the leading error terms, Φ_{xx} and Φ_{yy}, the rates of error reduction take exactly the order of two.

In a square domain of unit length, the analytic solution for the equation

$$\left(x+\frac{1}{2}\right)^{-1}\Phi_x + \left(y+\frac{1}{2}\right)^{-1}\Phi_y - \mu(\Phi_{xx} + \Phi_{yy}) = 0 \tag{7}$$

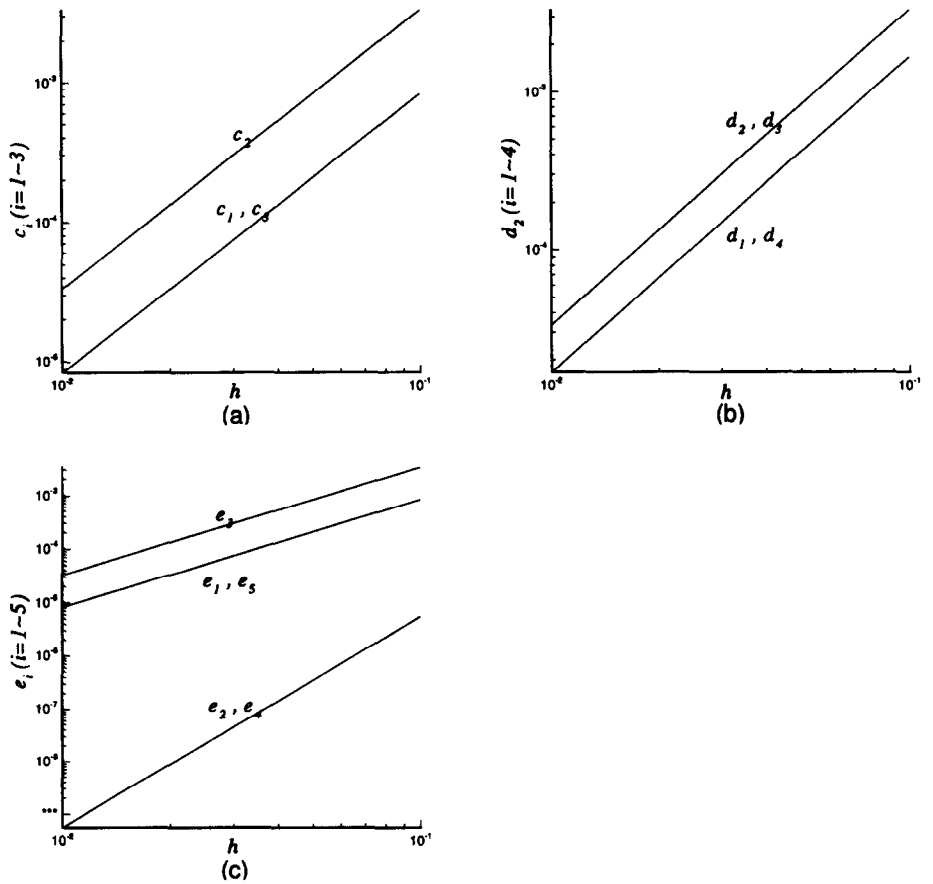

Fig. 2. The computed rates of coefficients appearing in Eq. (6). (a) Φ_{xx}, Φ_{xy}, Φ_{yy}; (b) Φ_{xxx}, Φ_{xxy}, Φ_{xyy}, Φ_{yyy}; (c) Φ_{xxxx}, Φ_{xxxy}, Φ_{xxyy}, Φ_{xyyy}, Φ_{yyyy}.

exists and takes the following form:

$$\Phi = \left(x + \frac{1}{2}\right)^2 + \left(y + \frac{1}{2}\right)^2 . \tag{8}$$

The performance of finite element methods is usually assessed on the basis of global error measured in an integral form. By substituting the analytic solution into Eq. (6), we can obtain the L_2-norms for the discretization error T:

$$\mathrm{err}(\Phi) = \sqrt{\left(\frac{\sum (\Phi_{\mathrm{exact}} - \hat{\Phi})^2}{n}\right)} ,$$

where n is the total number of nodal points on the computational domain. Here, Φ_{exact} and $\hat{\Phi}$ denote the exact solution and the computed finite element solution, respectively.

To gain insight into the error reduction sequences, refinement of grid spacings is required along each dimension. Solutions to the problem under consideration were computed from several uniform grids. Starting from 5×5, we continue to double the number of nodal points along each dimension. For completeness, we benchmark the scheme performance in terms of the rate of convergence defined as

$$\mathrm{rate} = \frac{\log\left(\frac{\mathrm{err}_1}{\mathrm{err}_2}\right)}{\log\left(\frac{n_2}{n_1}\right)} .$$

err_1 and err_2 are computed errors which are obtained on the basis of n_1 and n_2 total nodal points and tabulated in Table 1. The error norms thus obtained enable us to estimate the resulting rate of convergence.

When faced with multi-dimensional transport equations, it is of importance to know the variations of discretization errors along and normal to the flow directions against the flow angle $\theta = \tan^{-1}(v/u)$. To accomplish this task, we further transform T in Eq. (6) from the physical coordinates (x, y) to the streamline coordinate s and its normal n through one-to-one mapping. Application of the chain rule yields

$$T = C_1(h, \theta)\Phi_{ss} + C_2(h, \theta)\Phi_{sn} + C_3(h, \theta)\Phi_{nn} + \cdots , \tag{9}$$

where h is the uniform grid size.

Similar to the derivation of coefficients in Eq. (6), to gain access to C_1, C_2 and C_3 is also mathematically complicated. It is, as a consequence, appropriate to represent artificial viscosities graphically against θ and h. As seen in Fig. 3, we are aware that the physically correct artificial viscosity has been added implicitly along the streamline. This implies that the discrete system has been stabilized, at least, along the flow direction. Extreme values occur at the flow directions 45° and 135°. It is worthwhile to note that when the analysis is performed in a one-dimensional-like context ($\theta = 0°, 90°$), the truncation error remains only along the streamline direction. In circumstances when the value of C_2 is locally equal to zero, the resulting scheme is by no means unconditionally stable owing to the positive value of C_1 and negative value of C_3.

Table 1
Rate of convergence for the test problem defined in Eqs. (7) and (8) using the proposed discretized advection–diffusion scheme

Element	L_2-norm	Convergence rate
5×5	3.2614×10^{-3}	3.36
10×10	3.1738×10^{-4}	3.19
20×20	3.4681×10^{-5}	3.29
40×40	3.5297×10^{-6}	

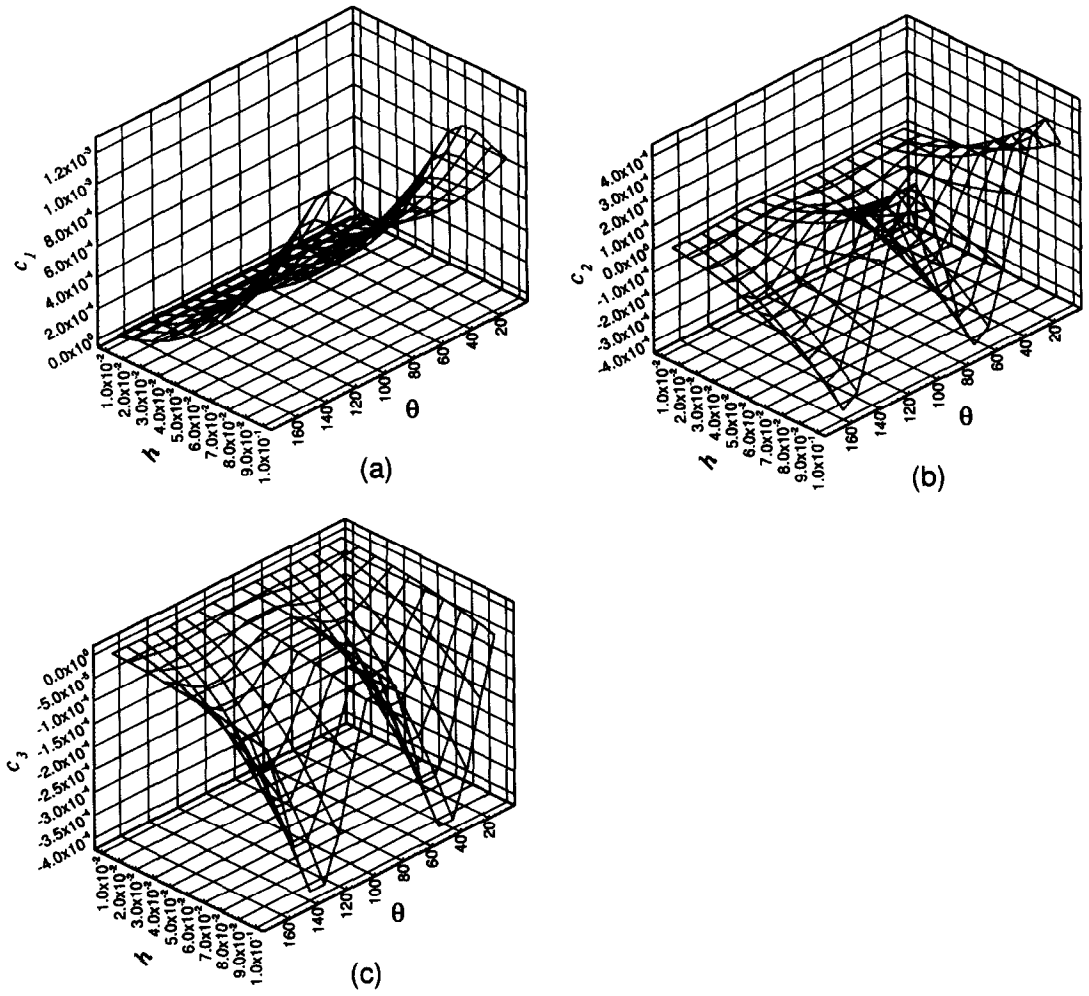

Fig. 3. The computed coefficients of C_i ($i = 1$–3) in Eq. (9) against the grid size h and the flow angle θ. (a) C_1; (b) C_2; (c) C_3.

2.4. Fundamental study on monotonicity

As the flow convection largely dominates diffusion, it is common to encounter a boundary layer like solution profile. In such extreme circumstance, classical upwind finite element methods often fail to resolve oscillatory solutions in regions where steep gradients exist. In this regard, the selection of a legitimate test space that is applicable to the present framework is in great need. Applying the test space considered in the present framework, we integrate the convection–diffusion equation by using the bilinear element to render the local matrix for each element. In a block of four bilinear elements, an algebraic equation for the grid node (i, j), as shown in Fig. 4 for example, can be formulated by assembling local matrices of neighboring four bilinear elements. To this end, we derive and represent the discrete finite element equation in a form similar to that expressed in the finite difference setting:

$$\sum_{i=1}^{9} a_i \Phi_i = 0 . \tag{10}$$

The mathematical effort in deriving above coefficients $a_i = a_i(\mathrm{Pe}_x, \mathrm{Pe}_y, h)$ is considerable. These coefficients are worth calculating because they help us to decide under what conditions the coefficient

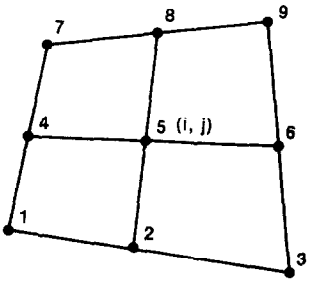

Fig. 4. Description of the derivation of coefficients in Eq. (10) for a pack of four elements with the common index (i, j) (Point 5).

matrix can be classified as irreducible diagonally dominant, as defined in Definition 1. As aided by the theorems given in Section 2.2, we can define the monotonic region from the signs of a_i. By varying the values of Pe_x against Pe_y, we designate the shaded area in Fig. 5 as stable since this allows us to gain access to the monotonic solution through the underlying concept of the M-matrix which is given in Section 2.2. Subject to this stability constraint condition, there is an upper limit on the allowable Peclet number above which the finite element solution deteriorates. Consideration will be specifically given later on to making compensation for this drawback. Of note is that as this analysis is reduced to one dimension, the discretization equation turns out to be exactly the localized adjoint method of Celia [12]. When joined with the accessible consistency property discussed in Section 2.3, we can expect to obtain the convergence solution as long as the pairwise Peclet numbers Pe_x and Pe_y fall in the realm of the stable region.

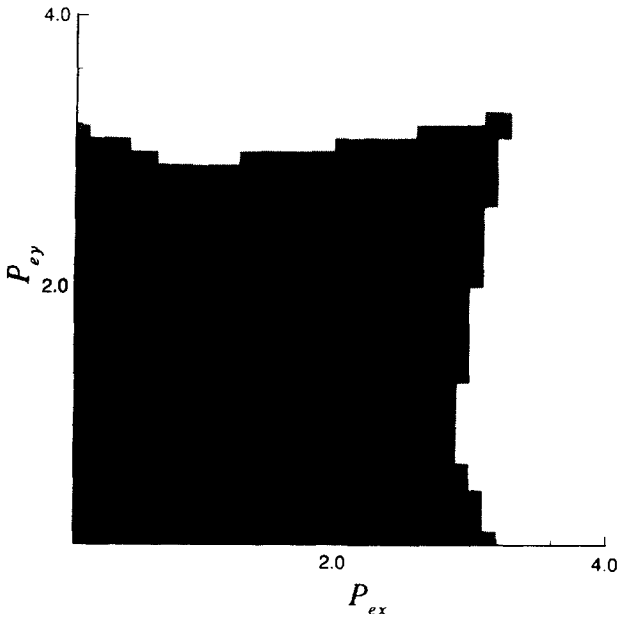

Fig. 5. Illustration of the shaded monotonic region underlying the proposed upwind scheme.

3. Refinement on monotonicity-preservation upwind model

3.1. Unconditionally monotonic flux discretization scheme

While monotonic finite element solutions of Eq. (1) are available as discussed in Section 2.4, the restriction of using Peclet numbers in a limited range precludes the extension of the proposed model to a wider scope of applications. In order to remove this constraint, we bring in the concept of the method of characteristics because the higher the Peclet numbers are, the more the differential system tends to be hyperbolic. For a given interior spatial point, physical reasoning suggests us not to take each stiffness matrix involving this point into consideration in the assemblage procedures. Instead of four elements, we only consider the element upstream of this point in mimicking the characteristic behavior. To demonstrate the feasibility of this characteristic extension, we will present the results of a benchmark test problem in the result section.

3.2. Test functions spanned by Legendre polynomials

In the weak form of the weighted residuals statement for Eq. (1), two integrals, namely $\int_{\Omega^e} W_i N_{j,\underline{X}}\, d\Omega^e$ and $\int_{\Omega^e} W_{i,\underline{X}} N_{j,\underline{X}}\, d\Omega^e$, need to be evaluated in rendering the stiffness matrix equation. Here, $(\cdot)_{,\underline{X}}$ denotes the partial differentiation of $(\cdot)$ with respect to x and y. The inclusion of the exponential function makes these integrals very expensive to compute because the order of the corresponding polynomial integrands tends to be infinitely high, as evidenced by the following identify:

$$e^{\gamma} = 1 + \gamma + \frac{\gamma^2}{2!} + \frac{\gamma^3}{3!} + \cdots + \frac{\gamma^n}{n!} + \cdots \quad ; -\infty < \gamma < \infty .$$

In recognizing this fact, a fundamental impediment to the utilization of exponential weighting functions becomes clear in the course of performing area integration. It is these integrands of infinite polynomial order that forbid the effective use of an exponential weighting function to obtain finite element solutions because the adequate number of Gaussian integration points is also conceptually infinite. While the proposed upwind scheme yields a monotonic solution irrespective of the Peclet number, there is considerable computational expense in dealing with the indispensable finite element integration. This is the main reason why we have to introduce Legendre polynomials to reduce the number of integration points needed.

In the first place, we rewrite the shape and weighting functions in terms of Legendre polynomials:

$$\begin{aligned} &P_0(t) = 1 , \\ &P_1(t) = t , \\ &P_2(t) = \frac{1}{2}(3t^2 - 1) , \\ &P_3(t) = \frac{1}{2}(5t^3 - 3t) , \\ &\quad\vdots \\ &\text{etc.} \end{aligned} \tag{11}$$

Without a potential loss of accuracy when transforming the polynomial basis space to the Legendre functional space, N_i shown in Eq. (4) can be expressed as

$$N_i = \frac{1}{4}[P_0(\xi) + \xi_i P_1(\xi)][P_0(\eta) + \eta_i P_1(\eta)] . \tag{12}$$

Just as the shape function redefined according to Eq. (12), more mathematically complicated weighting functions W_i can be also analytically expressed by the following infinite series:

$$
\begin{aligned}
W_i &= D_i W_\xi(\xi) W_\eta(\eta)\,, \\
&= D_i \sum_{n=0}^{x} d_{\xi_n} P_n(\xi) \sum_{n=0}^{y} d_{\eta_n} P_n(\eta)\,, \\
W_{i,\xi} &= D_i W'_\xi(\xi) W_\eta(\eta)\,, \\
&= D_i \sum_{n=0}^{x} e_{\xi_n} P_n(\xi) \sum_{n=0}^{y} d_{\eta_n} P_n(\eta)\,, \\
W_{i,\eta} &= D_i W_\xi(\xi) W'_\eta(\eta)\,, \\
&= D_i \sum_{n=0}^{x} d_{\xi_n} P_n(\xi) \sum_{n=0}^{y} e_{\eta_n} P_n(\eta)\,,
\end{aligned}
\tag{13}
$$

where

$$
\begin{aligned}
D_i &= \frac{1}{4} \exp\left(\frac{u h_\xi \xi_i}{2\mu}\right) \exp\left(\frac{v h_\eta \eta_i}{2\mu}\right), \\
W_\xi(\xi) &= (1 + \xi_i \xi) \exp\left(-\frac{u h_\xi \xi}{2\mu}\right), \\
W_\eta(\eta) &= (1 + \eta_i \eta) \exp\left(-\frac{v h_\eta \eta}{2\mu}\right), \\
d_{\xi_n} &= \frac{2n+1}{2} \int_1 W_\xi(t) P_n(t)\, \mathrm{d}t\,, \\
d_{\eta_n} &= \frac{2n+1}{2} \int_{-1} W_\eta(t) P_n(t)\, \mathrm{d}t\,, \\
e_{\xi_n} &= \frac{2n+1}{2} \int_{-1} W'_\xi(t) P_n(t)\, \mathrm{d}t\,, \\
e_{\eta_n} &= \frac{2n+1}{2} \int_{-1} W'_\eta(t) P_n(t)\, \mathrm{d}t\,.
\end{aligned}
\tag{14}
$$

We then substitute Eqs. (12)–(14) into the weighted residuals statement for Eq. (1). By virtue of the orthogonal property given by

$$
\int_{-1}^{1} P_i(t) P_j(t)\, \mathrm{d}t = \frac{2}{2i+1} \delta_{ij} \quad (i \text{ is dummy index})\,. \tag{15}
$$

we can show that Legendre polynomials of higher order make no contribution to the integrals, such as $\int_{\Omega^e} W_{i,\underline{X}} N_{j,\underline{X}}\, \mathrm{d}\Omega^e$ and $\int_{\Omega^e} W_i N_{j,\underline{X}}\, \mathrm{d}\Omega^e$. The detailed proof is given in Appendix A. With the fact mentioned above, we are aware that the weighting function taking the form of Eqs. (13)–(14) is equivalent to

$$
W_i = D_i [d_{\xi_0} P_0(\xi) + d_{\xi_1} P_1(\xi)][d_{\eta_0} P_0(\eta) + d_{\eta_1} P_1(\eta)]\,, \tag{16}
$$

$$
W_{i,\xi} = D_i [e_{\xi_0} P_0(\xi) + e_{\xi_1} P_1(\xi)][d_{\eta_0} P_0(\eta) + d_{\eta_1} P_1(\eta)]\,, \tag{17}
$$

$$
W_{i,\eta} = D_i [d_{\xi_0} P_0(\xi) + d_{\xi_1} P_1(\xi)][e_{\eta_0} P_0(\eta) + e_{\eta_1} P_1(\eta)]\,. \tag{18}
$$

in a sense that the use of higher-order Legendre polynomials (13) or lower ones, defined in Eqs. (16), yields exactly the same stiffness matrix. A clear manifestation of the equivalence between two classes of polynomials makes the proposed scheme more attractive because along each spatial coordinate only two integration points are sufficient to yield exact integration. Considerable CPU time will be saved without loss of accuracy.

4. Numerical study

A finite element model, endowed with the monotonicity property, will be validated analytically through several advection–diffusion problems defined in two dimensions. For completeness, problems both with/without internal/boundary layers are selected for use in the present study.

4.1. Problem without a boundary layer

The first example we will deal with is that of a smoothly varying transport problem, as defined in Fig. 6. Subject to the boundary condition of the Dirichlet type, the analytic solution takes the following form if the velocity field is assumed to be constant, i.e. $\underline{u} = (1, 10.5)$:

$$\Phi = \frac{\Phi_0}{e^{r_+} - e^{r_-}} e^{\delta_x/2} \sin(\pi x)(e^{r+y} - e^{r-y}),$$

$$r_\pm = \frac{1}{2}\delta_y \pm \frac{1}{2}\sqrt{(\delta_y^2 + 4W)}, \qquad W = (4\pi^2 + \delta_x^2)/4,$$

where $\Phi_0 = 1$, $\delta_x = uL/\mu$, $\delta_y = vL/\mu$, $L = 1$ and $\mu = 1$.

The relative error obtained in a 15×15 uniformly discretized domain is 2.434×10^{-3}, as measured in terms of the so-called L_2-norm. For the purpose of making a comparison, we have also plotted the QUICK solution of Arampatzis and Assimacopoulos [13]. Indicative from Fig. 7 which plots prediction errors at $x = 0.5$, the largest predicted error occurs in the vicinity of $y = 1$ where higher solution gradients are observed, as seen in Fig. 8. This benchmark test demonstrates the advantage over the QUICK scheme in predicting solutions classified as high gradient type.

4.2. Problem with a boundary layer

The task of capturing a sharp profile in the physical domain has long been regarded as important. The test problem attempted here is subject to the boundary values specified in Fig. 9. The analytic solution to this problem involves the boundary layer and takes the following form:

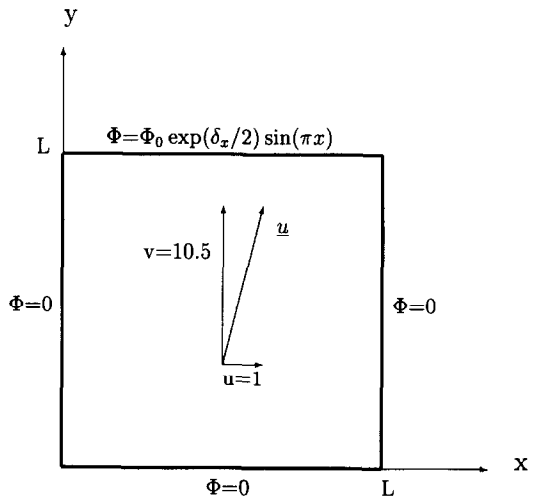

Fig. 6. Illustration of the test problem in Section 4.1.

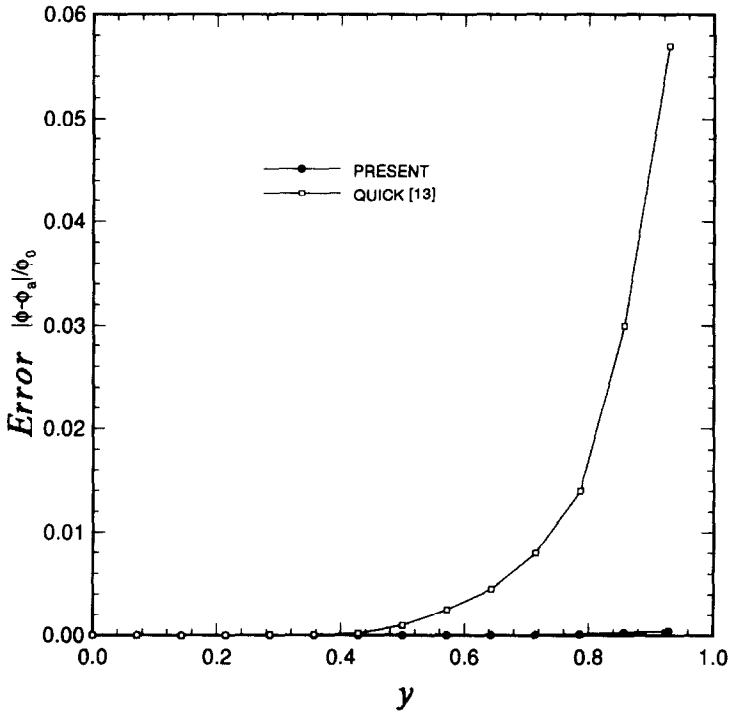

Fig. 7. A comparison of the computed solution profile at $x = 0.5$ for the test problem given in Section 4.1.

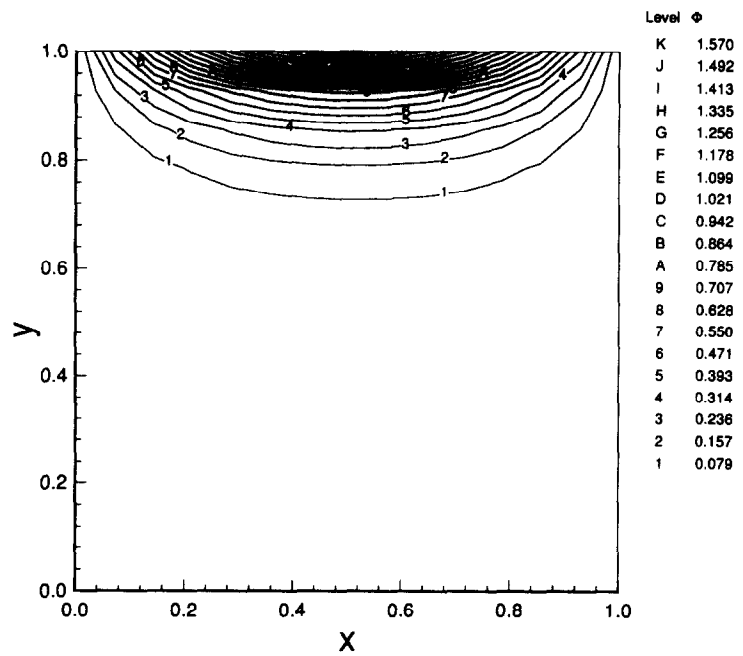

Fig. 8. Computed contour plots of Φ for the problem defined in Section 4.1.

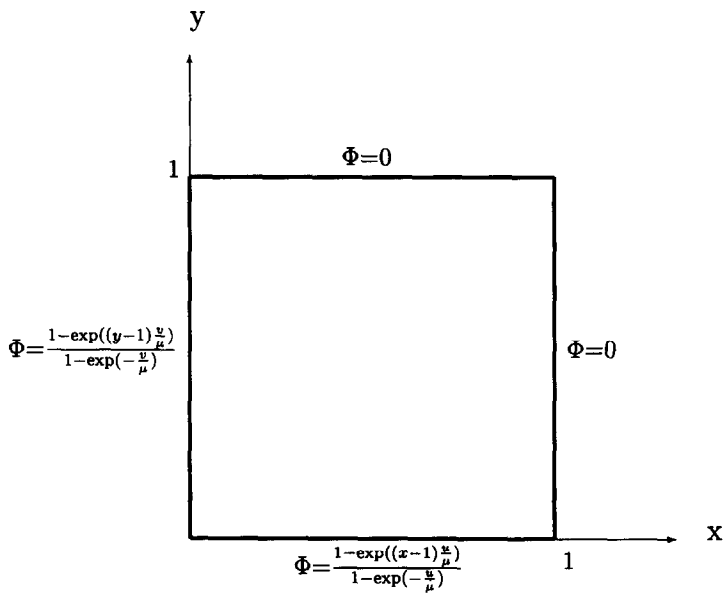

Fig. 9. Illustration of the test problem defined in Section 4.2.

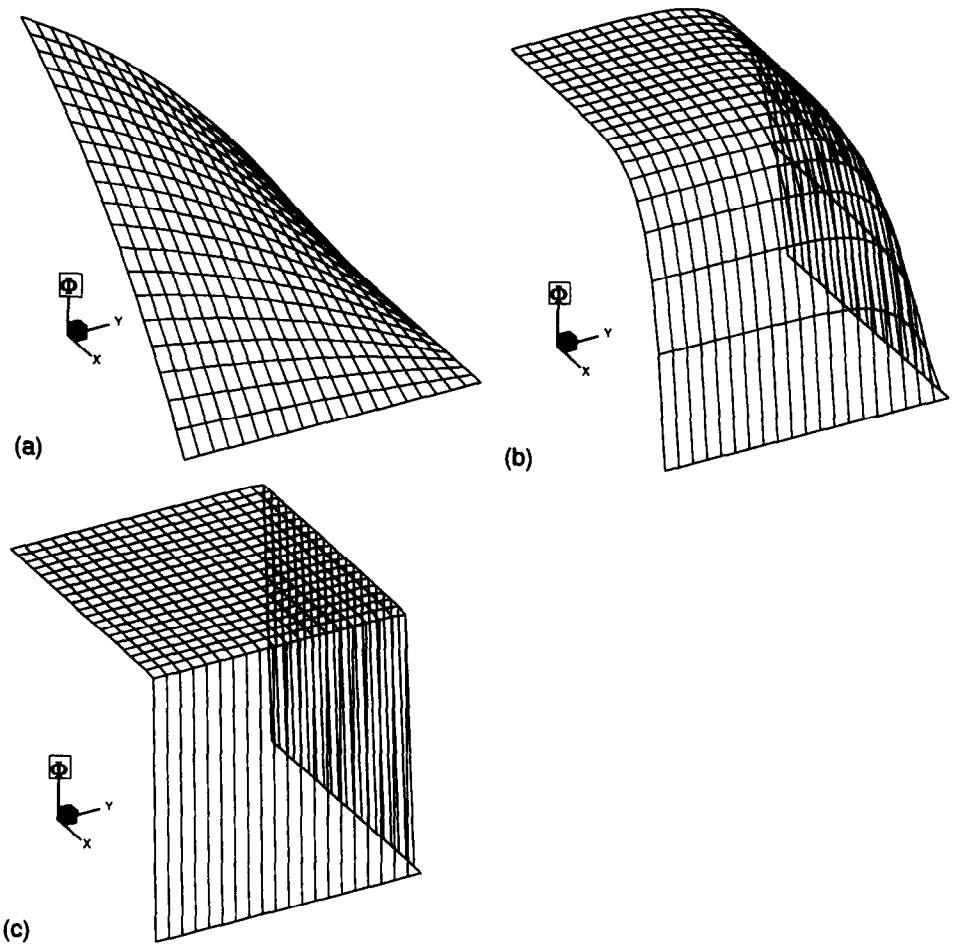

Fig. 10. Computed solution of Φ for the problem defined in Section 4.2. (a) $u = v = 1$; (b) $u = v = 10$; (c) $u = v = 100$.

Table 2
Computed L_2-norms at different flow conditions for the problem defined in Section 4.2

Element	$u = v = 1$	$u = v = 10$	$u = v = 100$
10×10	1.175×10^{-9}	1.217×10^{-9}	2.902×10^{-6}
20×20	9.600×10^{-10}	1.060×10^{-9}	2.781×10^{-8}
40×40	6.833×10^{-10}	7.551×10^{-10}	4.958×10^{-10}

$$\Phi(x, y) = \frac{\left[1 - \exp\left((x-1)\frac{u}{\mu}\right)\right]}{\left[1 - \exp\left(\frac{-u}{\mu}\right)\right]} \frac{\left[1 - \exp\left((y-1)\frac{v}{\mu}\right)\right]}{\left[1 - \exp\left(\frac{-v}{\mu}\right)\right]}.$$

Numerical solutions were sought on regular grids. Given the computed L_2-norm errors in Table 2, the present finite element formulation has ability to get around difficulties in association with a rapid change of solution, illustrated in Fig. 10, among the flow.

4.3. Skew advection–diffusion problem

An even harder problem which is distinguishable from the previous two test problems in its accommodation of an internal layer, will be considered. This test is that of the skewed flow transport problem which is regarded as a worst case scenario for any upwinding method [14]. In the square cavity of unit length, the cavity is divided into two subdomains by an inclined line passing through the corner point at $(0, 0)$ and having a slope of $m = \tan^{-1}(v/u)$. Throughout the whole domain, the magnitude of the velocity of interest is maintained as $q = \sqrt{u^2 + v^2} = 1$. Subject to the boundary condition for the working variable given in Fig. 11, a shear layer of high gradient or near discontinuity is expected when crossing the dividing line.

The objective of this case is to assess the merit and the deficiency of the proposed upwinding technique. We consider here the uniform flow, parallel to the dividing line, in a 20×20 uniformly discretized mesh, as shown in Fig. 12. Different diffusivities are considered which correspond to different degrees of advection dominance. With the diffusivity set to 1.67×10^{-2}, the cell Peclet number approaches 3 and falls into the monotonic regime. Finite element solutions shown in Fig. 12 are free of oscillations in regions close to as well as away from the dividing line. This is an indication that nonphysical spatial oscillations are not exhibited under certain conditions. With increasing Peclet numbers or decreasing diffusivities, poor performance for $\mu = 2 \times 10^{-3}$ makes such a method hardly applicable to problems involving steep gradients of the convected field variable Φ. There are two means

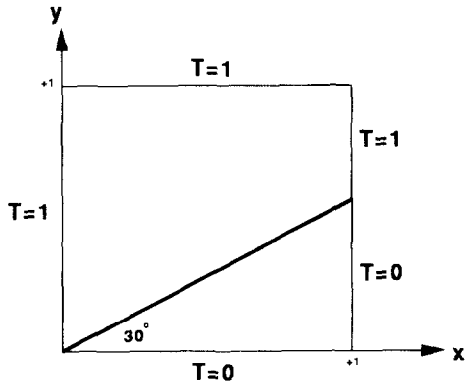

Fig. 11. Illustration of the skew advection–diffusion problem defined in Section 4.3.

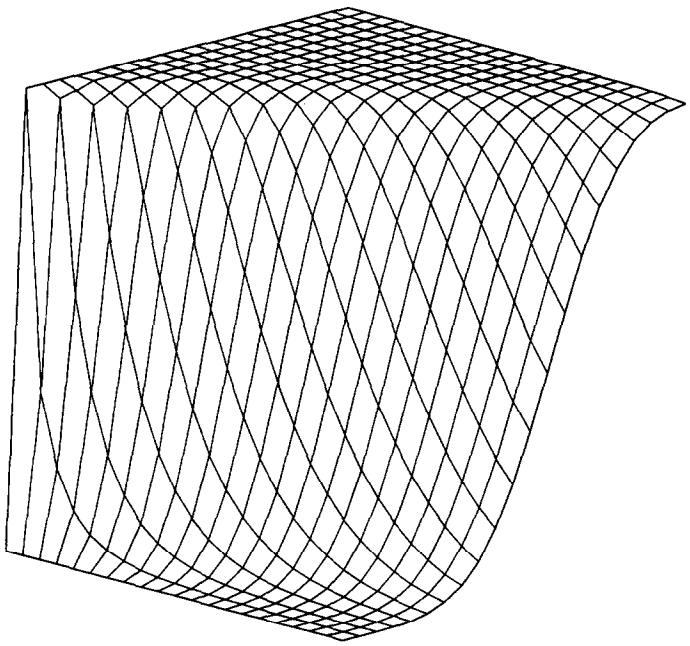

Fig. 12. Computed solution of Φ for the case of $\mu = 1.67 \times 10^{-2}$, which corresponds to the Peclet number falling into the monotonic region.

to avoid these wiggles. One can of course keep reducing the mesh size until the corresponding Peclet number falls into the category of the monotonic region in Fig. 13. There is, however, considerable computational expense associated with the frontal solver. This disadvantage makes practical computations infeasible. We thus turn to adopting other alternatives by activating the characteristic functionality to make the discrete system monotonic. In the presence of characteristic enhancement, the monotonic

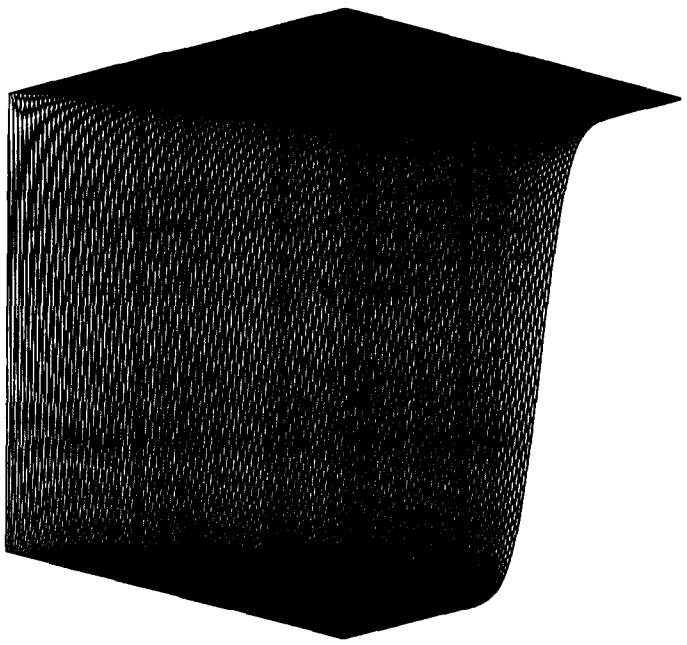

Fig. 13. Computed solution of Φ in a 150×150 uniformly discretized domain. The test considered is that of $\mu = 2 \times 10^{-3}$ which corresponds to Peclet numbers falling into the monotonic region.

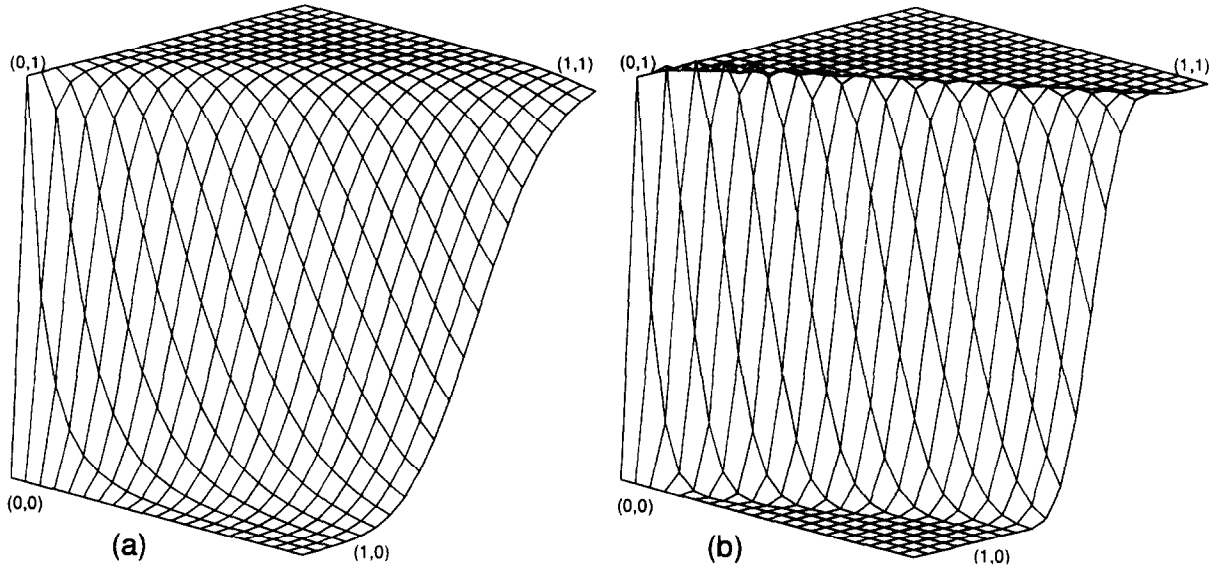

Fig. 14. Computed solution of Φ for the case of $\mu = 2 \times 10^{-3}$. (a) Characteristic version of the proposed finite element model; (b) characteristic-free finite element model.

solution for the case plotted in Fig. 13 can be also obtained at a domain with a much fewer nodal points. Fig. 14 is a clear illustration of the importance of incorporating the characteristic information into the proposed upwind finite element method. With the diffusivity set equal to 10^{-6}, the diffusion effects are virtually eliminated and the Peclet number approaches infinity. The case considered can be regarded as the conventional skew advection problem. A solution underlying the Legendre-polynomial-based characteristic upwind model is smoothly exhibited in Fig. 15(a). While these computed solutions in situations where convection significantly dominates diffusion are smoothly predicted, the quality of the analysis suffers from the problem of excessive numerical diffusion. In summary, the smeared solution shown in Fig. 15 is more or less representative of the outcome of using a method which is endowed with the M-matrix constraint condition.

4.4. *Advection–diffusion problem of Smith and Hutton*

The benchmark problem of Smith and Hutton [15] is of some importance, for it amounts to determining whether the finite element solution is sensitive to sharply varying inlet working variables. The test problem considered here is configured as an inflow–outflow transport problem. In the rectangular section, $-1 \leq x \leq 1, 0 \leq y \leq 1$ as shown in Fig. 16, a divergence-free velocity is prescribed by

$$u = 2y(1 - x^2),$$

$$v = -2x(1 - y^2).$$

Along the inlet of the test section, namely $-1 \leq x \leq 0$, $y = 0$, the working variable Φ is prescribed a priori as follows:

$$\Phi(-1 \leq x \leq 0,\ y = 0) = 1 + \tanh((2x + 1)10).$$

On the remaining boundaries $x = -1$, $y = 1$ and $x = 1$, working variables are specified by $\Phi = 1 - \tanh(10)$. The reason behind this specification is the fact that the compatible constraint condition demand transport field variables be little affected by the given velocity vector and diffusivity. On the outflow boundary, $0 \leq x \leq 1$, $y = 0$, Φ is coupled with the inner solution by specifying a zero gradient of Φ herein. This outflow boundary condition corresponds to allowing Φ to float.

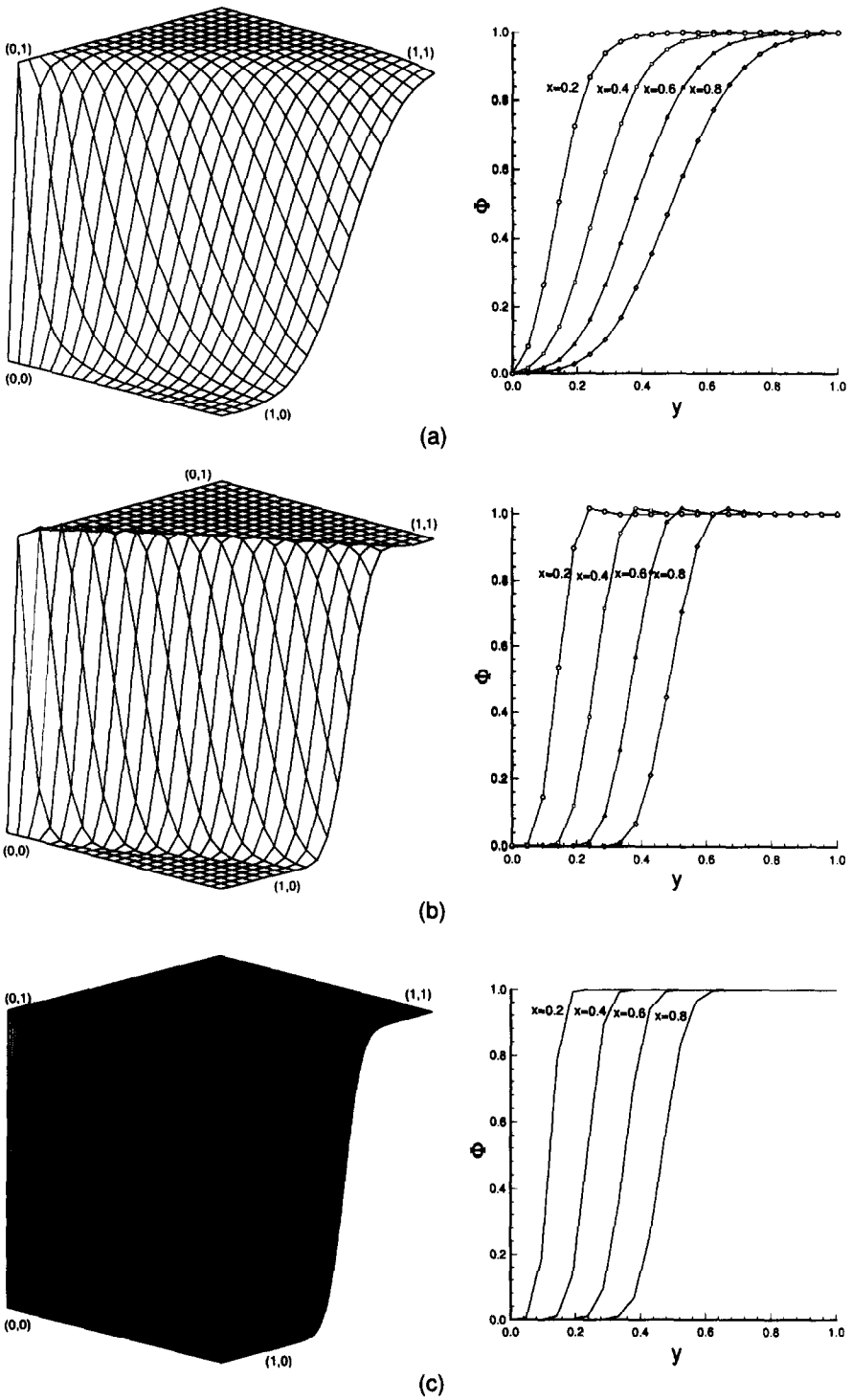

Fig. 15. Finite element solutions of Φ and their distributions at $x = \frac{1}{5}, \frac{2}{5}, \frac{3}{5}, \frac{4}{5}$. (a) Characteristic version implemented at 20×20 in the case of $\mu = 10^{-6}$; (b) characteristic-free version implemented at 20×20 in the case of $\mu = 2 \times 10^{-3}$; (c) characteristic-free version implemented at 150×150 in the case of $\mu = 2 \times 10^{-3}$.

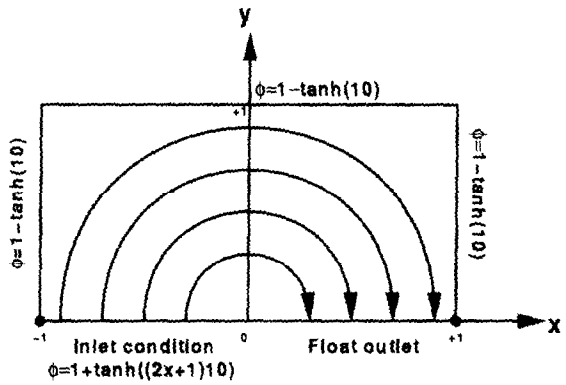

Fig. 16. Description of the test problem defined in Section 4.4.

In a fixed grid having spacings $\Delta x = \Delta y = 0.1$, the use of different values of μ yields different maximum Peclet numbers. Here, we consider $\mu = 10^{-6}$, 2×10^{-3}, 10^{-2} and 10^{-1} or max(Pe) = $(2 \times 10^5, 100, 20, 2)$. As evidenced by the computed solutions in Figs. 17 and 18, we can clearly demonstrate the effectiveness of the introduced characteristic weighting. Also of note is that oscillation-free solutions can be also rendered by using characteristic-free upwind model in a much refined grid shown in Fig. 19.

We summarize the effects of different Peclet numbers and grid resolutions for the cases considered in

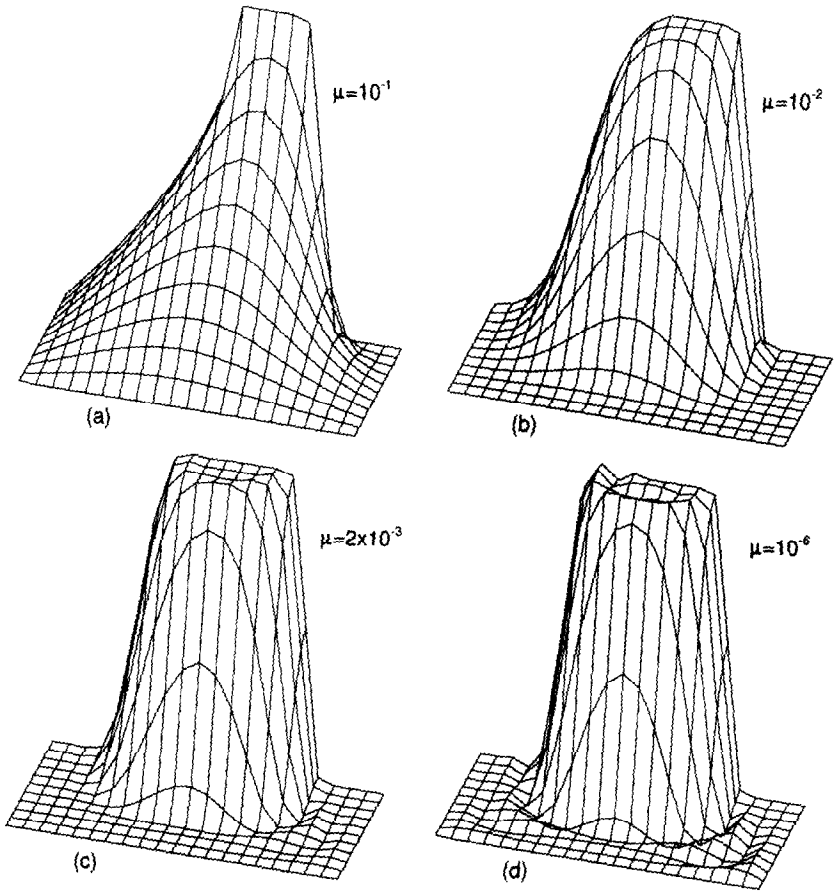

Fig. 17. Computed solution of Φ for problem defined in Section 4.4 using characteristic-free finite element model. (a) Pe = 2; (b) Pe = 20; (c) Pe = 100; (d) Pe = 2×10^5.

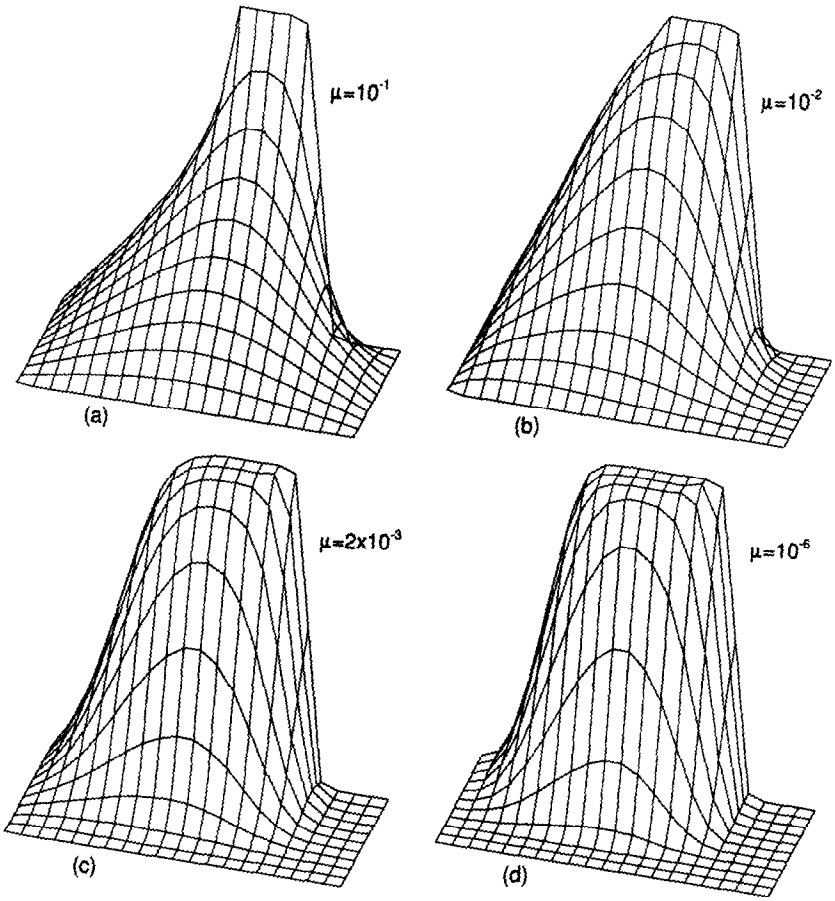

Fig. 18. Computed solution of Φ for problem defined in Section 4.4 using the characteristic version of the proposed finite element model. (a) Pe = 2; (b) Pe = 20; (c) Pe = 100; (d) Pe = 2×10^5.

this calculation by the computed finite element solutions at the outlet boundary in Fig. 20. Before closing this section, we would like to demonstrate the effectiveness of the proposed Legendre test space in Fig. 21. Apart from the commonly shared disk space, the use of Legendre polynomial can save three times of the disk space. We also plot CPU times against problem size in Fig. 21 to clarify the amount of extra CPU cost in dealing with 64 Gaussian integration points when using exponential weighting function; while only 4 integration points using the proposed Legendre polynomials.

5. Conclusions

(1) To stabilize the differential system under consideration, we have focused on developing a finite element method that is endowed with the upwinding property and an oscillation suppressant capability to suppress erroneous oscillations in the vicinity of high gradient. Thanks to the underlying M-matrix which is regarded as a means of resolving overshoots or undershoots, we can judiciously determine the degree of upwind-weighting a priori. We have endeavored to conduct basic studies, with the focus on numerical accuracy and stability. Through the modified equation analysis, considerable insight into the behavior of consistency property has been obtained. Most importantly, the employed monotonicity property is applicable to multiple dimensions. This finite element model has been rectified by solving analytic problems having different characters.

(2) Subject to limitations on the Peclet number, there is an upper bound on the allowable grid size, above which a monotonic solution is not accessible. The extension of the proposed upwinding model to the larger application range is made by taking the increasingly important characteristic

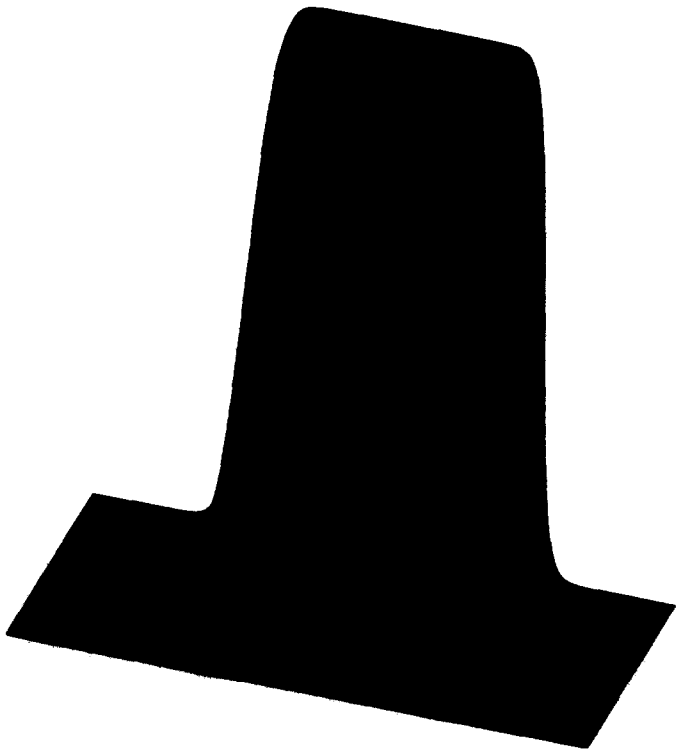

Fig. 19. Computed solution of Φ in a 200×100 uniform discretized domain for the test problem, given in Section 4.4, using the characteristic-free finite element model.

information into consideration. This serves as a cure for problems involving high Peclet numbers. To accomplish this, we have only considered element matrices upstream of the spatial point of interest. Inclusion of characteristic modification has effectively improved the monotonicity of the discrete solution, as seen from a clear manifestation of the predicted sharp profiles in the illustrative examples.

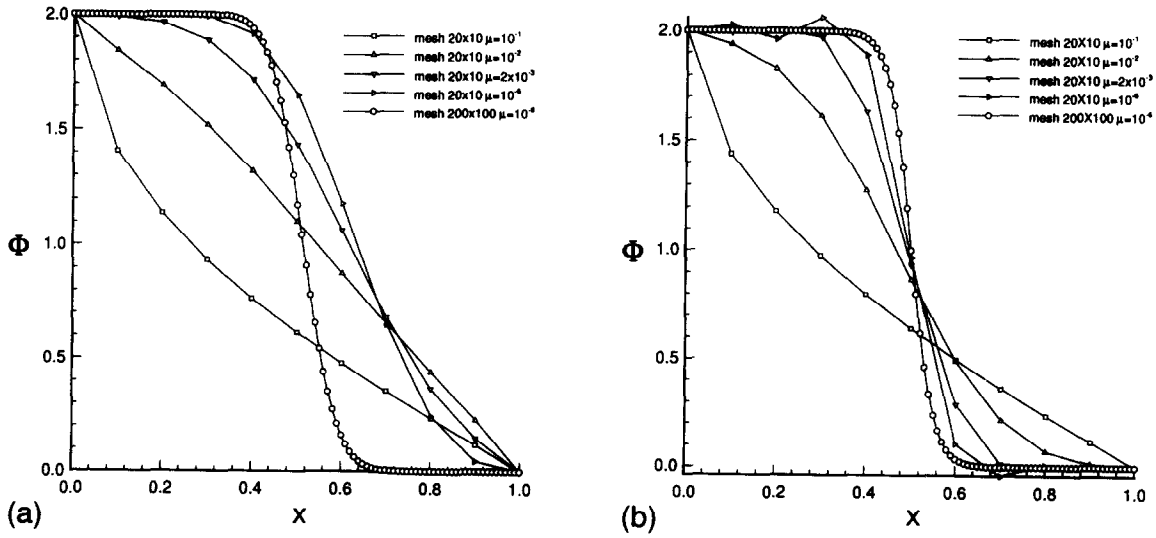

Fig. 20. The computed finite element solutions at the outlet boundary $0 \leq x \leq 1$, $y = 0$. (a) Characteristic version; (b) characteristic-free version.

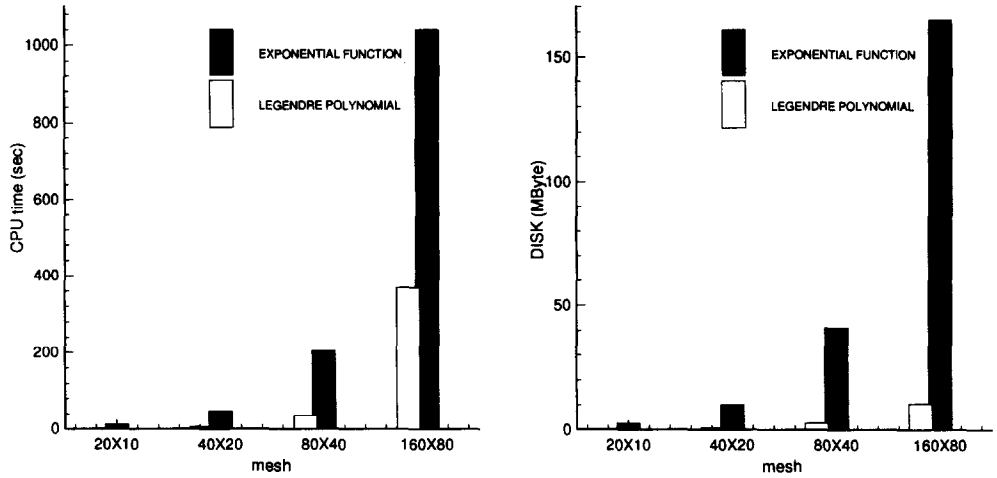

Fig. 21. Comparison of disk space and CPU time for the proposed upwind finite element model using the Legendre and exponential weighting function.

(3) Having obtained a high degree of robustness in the scheme stability, the finite element model proposed herein can serve as the numerical technique of choice for solving transport equations. A fundamental impediment to the direct application of this method in modelling engineering problems of practical relevance lies in its indispensable numerical integrations at the element level. To make the proposed scheme more applicable to large-size problems, we must rewrite the basis and test functions in terms of Legendre polynomials. The inherent orthogonal property, namely $\int_{-1}^{+1} P_i(t)P_j(t)\,\mathrm{d}t = 2/(2i+1)\delta_{ij}$, enables us to carry out the integral exactly using only two Gaussian integration points along each spatial direction. Also of note is that the utilization of Legendre polynomials enables the proposed scheme to be more amenable to fundamental studies, without loss a bit of monotonic behavior.

Appendix A

Following the weak formulation, the weighted residuals statement for Eq. (1) takes the following form:

$$\int_\Omega [W(u\Phi_{,x} + v\Phi_{,y}) + \mu(W_{,x}\Phi_{,x} + W_{,y}\Phi_{,y})]\,\mathrm{d}\Omega = 0\,. \tag{A.1}$$

There exist two kinds of integrals, namely $\int_\Omega W\Phi_{,\underline{X}}\,\mathrm{d}\Omega$ and $\int_\Omega W_{,\underline{X}}\Phi_{,\underline{X}}\,\mathrm{d}\Omega$, where $\underline{X}$ denotes the global coordinates x and y.

Transforming the global coordinates (x, y) to the local coordinates (ξ, η), these integrals can be rewritten as follows:

$$\int_\Omega W\Phi_{,x}\,\mathrm{d}\Omega = \int_{-1}^{1}\int_{-1}^{1} W(\Phi_{,\xi}\xi_{,x} + \Phi_{,\eta}\eta_{,x})|\boldsymbol{J}|\,\mathrm{d}\xi\,\mathrm{d}\eta\,, \tag{A.2}$$

$$\int_\Omega W\Phi_{,y}\,\mathrm{d}\Omega = \int_{-1}^{1}\int_{-1}^{1} W(\Phi_{,\xi}\xi_{,y} + \Phi_{,\eta}\eta_{,y})|\boldsymbol{J}|\,\mathrm{d}\xi\,\mathrm{d}\eta\,, \tag{A.3}$$

$$\int_\Omega W_{,x}\Phi_{,x}\,\mathrm{d}\Omega = \int_{-1}^{1}\int_{-1}^{1} (W_{,\xi}\xi_{,x} + W_{,\eta}\eta_{,x})(\Phi_{,\xi}\xi_{,x} + \Phi_{,\eta}\eta_{,x})|\boldsymbol{J}|\,\mathrm{d}\xi\,\mathrm{d}\eta\,, \tag{A.4}$$

$$\int_\Omega W_{,y}\Phi_{,y}\,\mathrm{d}\Omega = \int_{-1}^{1}\int_{-1}^{1} (W_{,\xi}\xi_{,y} + W_{,\eta}\eta_{,y})(\Phi_{,\xi}\xi_{,y} + \Phi_{,\eta}\eta_{,y})|\boldsymbol{J}|\,\mathrm{d}\xi\,\mathrm{d}\eta\,, \tag{A.5}$$

where $\boldsymbol{J} = \partial(x, y)/\partial(\xi, \eta)$ and $|\boldsymbol{J}| = \det(\boldsymbol{J})$.

The number of Gaussian integration points needed to carry out above integrations depends on the polynomial order of the integrand. For example, the order of integrand in $\int_\Omega W_{,x}\Phi_{,x}\,\mathrm{d}\Omega = \int_{-1}^{1}\int_{-1}^{1}(W_{,\xi}\xi_{,x}+W_{,\eta}\eta_{,x})(\Phi_{,\xi}\xi_{,x}+\Phi_{,\eta}\eta_{,x})|\boldsymbol{J}|\,\mathrm{d}\xi\,\mathrm{d}\eta$ is determined by $W_{,\xi}$, $W_{,\eta}$, $\Phi_{,\xi}$, $\Phi_{,\eta}$, $\xi_{,x}$, $\eta_{,x}$, and $|\boldsymbol{J}|$, where W is the weighting function, and Φ is interpolated by the bilinear shape function.

The coefficient matrix, $\boldsymbol{J}$, of the geometric transformation is generally a function of ξ,η. $\boldsymbol{J}$ could be a constant matrix only, if the affine transformation exists between local coordinates, (ξ,η), and global coordinates, (x, y). This implies that if the element shape is not too much distorted, $\boldsymbol{J}$ turns out to be a constant matrix. As a consequence, the polynomial orders of the integrand in Eqs. (A.2)–(A.5) are only dependent on W, Φ and the coordinate derivatives of W and Φ. The integrals need to be calculated are shown as following,

$$\int_{-1}^{1}\int_{-1}^{1} W\Phi_{,\xi}\,\mathrm{d}\xi\,\mathrm{d}\eta\,, \tag{A.6}$$

$$\int_{-1}^{1}\int_{-1}^{1} W\Phi_{,\eta}\,\mathrm{d}\xi\,\mathrm{d}\eta\,, \tag{A.7}$$

$$\int_{-1}^{1}\int_{-1}^{1} W_{,\xi}\Phi_{,\xi}\,\mathrm{d}\xi\,\mathrm{d}\eta\,, \tag{A.8}$$

$$\int_{-1}^{1}\int_{-1}^{1} W_{,\xi}\Phi_{,\eta}\,\mathrm{d}\xi\,\mathrm{d}\eta\,, \tag{A.9}$$

$$\int_{-1}^{1}\int_{-1}^{1} W_{,\eta}\Phi_{,\eta}\,\mathrm{d}\xi\,\mathrm{d}\eta\,, \tag{A.10}$$

where W and Φ are replaced by the nodal weighting function, $W_i(\xi,\eta)=\exp[-(uh_\xi)/2\mu(\xi-\xi_i)]\exp[-(vh_\eta)/2\mu(\eta-\eta_i)]N_i(\xi,\eta)$, and by the nodal shape function, $N_i(\xi,\eta)=\frac{1}{4}(1+\xi_i\xi)(1+\eta_i\eta)$, respectively.

The infinite polynomial order of W causes the order of integrand in Eq. (A.6)–(A.10) to be infinitely large. This fact demands the use of infinite number of Gaussian integration points to properly calculate the values of these integrals. This difficulty can be improved by transferring W and Φ to the orthogonal Legendre polynomial bases, $P_i(t)$, where $P_i(t)=(1/2^i i!)(\mathrm{d}^i/\mathrm{d}t^i)(t^2-1)^i$ and $\int_{-1}^{1}P_i(t)P_j(t)\,\mathrm{d}t = 2/(2i+1)\delta_{ij}$.

Firstly, we transfer the shape and weighting functions to the orthogonal polynomial bases, as shown in the following,

$$\begin{aligned} N_i(\xi,\eta) &= \frac{1}{4}(1+\xi_i\xi)(1+\eta_i\eta)\,,\\ &= \frac{1}{4}[P_0(\xi)+\xi_iP_1(\xi)][P_0(\eta)+\eta_iP_1(\eta)]\,, \end{aligned} \tag{A.11}$$

and

$$\begin{aligned} W_i &= D_iW_\xi(\xi)W_\eta(\eta)\,,\\ &= D_i\sum_{n=0}^{r} d_{\xi_n}P_n(\xi)\sum_{n=0}^{r} d_{\eta_n}P_n(\eta)\,,\\ W_{i,\xi} &= D_iW'_\xi(\xi)W_\eta(\eta)\,,\\ &= D_i\sum_{n=0}^{\infty} e_{\xi_n}P_n(\xi)\sum_{n=0}^{r} d_{\eta_n}P_n(\eta)\,,\\ W_{i,\eta} &= D_iW_\xi(\xi)W'_\eta(\eta)\,,\\ &= D_i\sum_{n=0}^{r} d_{\xi_n}P_n(\xi)\sum_{n=0}^{\infty} e_{\eta_n}P_n(\eta)\,, \end{aligned} \tag{A.12}$$

where

$$D_i = \frac{1}{4}\exp\left(\frac{uh_\xi \xi_i}{2\mu}\right)\exp\left(\frac{vh_\eta \eta_i}{2\mu}\right),$$

$$W_\xi(\xi) = (1+\xi_i\xi)\exp\left(-\frac{uh_\xi \xi}{2\mu}\right),$$

$$W_\eta(\eta) = (1+\eta_i\eta)\exp\left(-\frac{vh_\eta \eta}{2\mu}\right),$$

$$d_{\xi_n} = \frac{2n+1}{2}\int_{-1}^{1} W_\xi(t)P_n(t)\,\mathrm{d}t, \tag{A.13}$$

$$d_{\eta_n} = \frac{2n+1}{2}\int_{-1}^{1} W_\eta(t)P_n(t)\,\mathrm{d}t,$$

$$e_{\xi_n} = \frac{2n+1}{2}\int_{-1}^{1} W'_\xi(t)P_n(t)\,\mathrm{d}t,$$

$$e_{\eta_n} = \frac{2n+1}{2}\int_{-1}^{1} W'_\eta(t)P_n(t)\,\mathrm{d}t,$$

Substituting these shape and weighting functions in the context of the orthogonal Legendre polynomial bases into Eqs. (A.6)–(A.10), we can dispense with the higher-order polynomials by virtue of orthogonal property. For example,

$$\begin{aligned}
&\int_{-1}^{1}\int_{-1}^{1} W_i N_{j,\xi}\,\mathrm{d}\xi\,\mathrm{d}\eta \\
&= \int_{-1}^{1}\int_{-1}^{1}\left[D_i\sum_{n=0}^{\infty} d_{\xi_n}P_n(\xi)\sum_{n=0}^{\infty} d_{\eta_n}P_n(\eta)\right]\frac{\mathrm{d}}{\mathrm{d}\xi}\left\{\frac{1}{4}[P_0(\xi)+\xi_jP_1(\xi)][P_0(\eta)+\eta_jP_1(\eta)]\right\}\mathrm{d}\xi\,\mathrm{d}\eta \\
&= \int_{-1}^{1}\int_{-1}^{1} D_i[d_{\xi_0}P_0(\xi)+d_{\xi_1}P_1(\xi)][d_{\eta_0}P_0(\eta)+d_{\eta_1}P_1(\eta)] \\
&\quad \frac{\mathrm{d}}{\mathrm{d}\xi}\left\{\frac{1}{4}[P_0(\xi)+\xi_jP_1(\xi)][P_0(\eta)+\eta_jP_1(\eta)]\right\}\mathrm{d}\xi\,\mathrm{d}\eta.
\end{aligned} \tag{A.14}$$

With the fact mentioned above, we can use the following equivalent weighting functions to yield

$$W_i = D_i[d_{\xi_0}P_0(\xi)+d_{\xi_1}P_1(\xi)][d_{\eta_0}P_0(\eta)+d_{\eta_1}P_1(\eta)], \tag{A.15}$$

$$W_{i,\xi} = D_i[e_{\xi_0}P_0(\xi)+e_{\xi_1}P_1(\xi)][d_{\eta_0}P_0(\eta)+d_{\eta_1}P_1(\eta)], \tag{A.16}$$

$$W_{i,\eta} = D_i[d_{\xi_0}P_0(\xi)+d_{\xi_1}P_1(\xi)][e_{\eta_0}P_0(\eta)+e_{\eta_1}P_1(\eta)], \tag{A.17}$$

References

[1] G.D. Raithby and K.E. Torrance, Upstream-weighted differencing scheme and their application to elliptic problems involving fluid flow, Comput. Fluid 2 (1974) 191–206.

[2] B.P. Leonard, A stable and accurate convective modelling procedure based on quadratic upstream intepolation, Comput. Methods Appl. Mech. Engrg. 19 (1979) 59–98.

[3] T.J.R. Hughes and A.A. Brooks, A multidimensional upwind scheme with no crosswind diffusion, in: T.J.R. Hughes, ed., Finite Element Methods for Convection Dominated Flows (ASME, New York, 1979).

[4] A. Mizukami and T.J.R. Hughes, A Petrov–Galerkin finite element method for convection dominated flow: An accurate upwinding technique for satisfying the maximum principle, Comput. Methods Appl. Mech. Engrg. 50 (1985) 181–193.

[5] M. Ahués and M. Telias, Petrov–Galerkin scheme for the steady state convection–diffusion equation, Finite Elem. Water Res. 2(3-2) (1982) 12.

[6] T. Meis and U. Marcowitz, Numerical solution of partial differential equations, Applied Mathematical Sciences, Vol. 32 (Springer-Verlag, New York, 1981).

[7] T. Ikeda, Maximum principle in finite element models for convection–diffusion phenomena, in: Lecture Notes in Numerical and Applied Analysis, Vol. 4 (North-Holland, Amsterdam, 1983).
[8] J.G. Rice and R.J. Schnipke, A monotone streamline upwind finite element methods for convection-dominated flows, Comput. Methods. Appl. Mech. Engrg. 47 (1984) 313–327.
[9] D.L. Hill and E.A. Baskharone, A monotone streamline upwind method for quadratic finite elements, Int. J. Numer. Methods Fluids 17 (1993) 463–475.
[10] M.D. Gunzburger, Finite Element Methods for Viscous Incompressible Flows (Academic Press, 1989).
[11] R.F. Warming and B.J. Hyett, The modified equation approach to the stability and accuracy analysis of finite-difference method, J. Comput. Phys. 14 (1974) 159–179.
[12] M.A. Celia and W.G. Cray, Numerical Methods for Differential Equations (Prentice-Hall, Englewood Cliffs, NJ, 1992).
[13] G. Arampatzis and D. Assimacopoulos, Treatment of numerical diffusion in strong convective flows, Int. J. Numer. Methods Fluids 18 (1994) 313–331.
[14] D.F. Griffiths and A.R. Mitchell, in: T.J.R. Hughes, ed., Finite Element for Convection Dominated Flows, AMD, Vol. 34 (ASME, New York, 1979) 91–104.
[15] R.M. Smith and A.G. Hutton, The numerical treatment of convection—a performance comparison of current methods, Int. J. Numer. Methods Heat Trans. 5 (1982) 439–461.